

# *In vivo* detection of reduced scattering coefficient of C6 glioma in rat brain tissue by near-infrared spectroscopy

Lijuan Dai  
Zhiyu Qian

Nanjing University of Aeronautics and Astronautics  
Department of Biomedical Engineering  
No. 29 Yuado Street  
Nanjing, Jiangsu 210016, China

Kuanzheng Li  
Tianming Yang

Southeast University  
College of Medicine  
Nanjing, Jiangsu 210009, China

Huinan Wang

Nanjing University of Aeronautics and Astronautics  
Department of Biomedical Engineering  
No. 29 Yuado Street  
Nanjing, Jiangsu 210016, China

**Abstract.** The purpose of this study is to investigate the reduced scattering coefficient of C6 glioma by the near-infrared (NIR) technique. Light scattering properties of C6 glioma in brain tissue is measured by NIR spectroscopy within the wavelength range from 700 to 850 nm. C6 gliomas were implanted in rats' right brains. The scattering properties of the left and right target corresponding to the position of normal and tumor tissue were measured by a bifurcated needle probe on postoperative days 3, 10, and 17. The results show that there was no significant difference in reduced scattering coefficient between left and right brain tissue at postoperative day 3, but significant decreases were found between left and right brains at postoperative days 10 and 17. This study proved our initial hypothesis that the NIR technique may have a potential for clinical application in brain  $\mu$ glioma diagnosis. © 2008 Society of Photo-Optical Instrumentation Engineers. [DOI: 10.1117/1.2957974]

Keywords: C6 glioma; tumor; near-infrared spectroscopy.

Paper 07263R received Jul. 19, 2007; revised manuscript received Jan. 21, 2008; accepted for publication Mar. 12, 2008; published online Aug. 8, 2008.

## 1 Introduction

Gliomas are a group of multiform, accumulative tumors that appear in the neuroectoderm. They generally induce perifocal edema and a massive increase of intracranial pressure for their compression, infiltration, and destruction on brain tissues. The C6 rat intracerebral glioma model is prevalent in glioma research for its good growth yields and low mortality rate. Perifocal inflamed symptoms and neonatal blood vessels occur at postoperative day (POD) 5. On POD 10, tumors increase highly in size with cellular exponential growth. During days 15–20, tumors reveal malignant gliomas with intratumoral hemorrhage and necrosis.<sup>1–4</sup>

Presently, near infrared spectroscopy is used widely in the differentiation tissue types.<sup>5,6</sup> It is known that near-infrared (NIR) light in the 700–850 nm wavelength range is special to tissues as light scattering is more prominent than light absorption. There is a significant difference in light-scattering properties between different tissue types and between healthy and diseased tissues due to their differences in anatomical substructure; cellular and intracellular organelles of diseased tissues undergo changes in their density, morphological size, and shape.<sup>6–9</sup> In this study, an effort was made to develop NIR technology as an alternate method for detection of certain characteristics of glioma.

The aim of this study is to determine the light-scattering patterns from rat cerebral glioma by using NIR reflectance spectroscopy. The C6 gliomas were induced in Sprague-

Dawley rats (SD) by the stereotactic implantation technique.<sup>10</sup> It has been reported that tumors generally have a lower scattering coefficient measured *in vitro* than normal tissue.<sup>7,9</sup> Therefore, for this study, our hypothesis is that gliomas will lead to a decrease in light scattering of the brain and can be differentiated by the *in vivo* NIR measurement.

## 2 Materials and Methods

### 2.1 Cell Cultivation

The C6 glioma cells were grown in RPMI 1640 medium supplemented with 10% fetal calf serum (FCS), 2 mM L-glutamine, 50  $\mu$ g/mL streptomycin, and 50 U/mL penicillin. Cells were maintained in an incubator with 5% CO<sub>2</sub>, 100% humidity at 37 °C. Before implantation to the rat brain, cells growing in an exponential rate were harvested by Trypsin for 5 min at 37 °C. Trypsin was inactivated by medium with 10% FCS, and the cells centrifuged at 600 g for 5 min. The pellets were then resuspended in RPMI 1640 medium without any supplement, at a concentration of 10<sup>6</sup> cells/ $\mu$ L. Gentle manual agitation was applied to keep the cells in suspension before implantation.

### 2.2 Implantation Surgery

Thirty adult male Sprague-Dawley rats (230–280 g, Southeast University vivarium) were used in this study. The animals were kept in their habitual environment until the day of the experiment. All animals were anesthetized with 4% Nembutal (40 mg/kg, i.p.) and mounted into a stereotactic frame (incisor bar 2.4 mm below the interaural line) in a flat-skull posi-

Address all correspondence to: Zhiyu Qian, Nanjing University Aeronautics and Astronautics, Department of Biomedical Engineering, No. 29 Yuado Street, Nanjing, Jiangsu 210016, China. Tel: 086-025-84891938-602; E-mail: zhiyu@nuaa.edu.cn

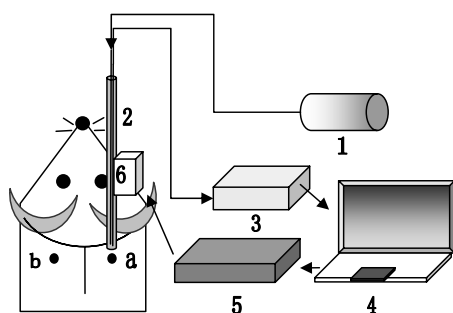


**Fig. 1** Diagram of the NIRS system for measurements on brain tissue. 1—5 W halogen lamp as the light source. 2—Optic probe containing two silica fibers. 3—USB2000 spectrometer. 4—Computer and software. 5—MID-7604 driver. 6—PCI-7344 controller and step motor, a—the point of implant hole and the projection C6 glioma and b—symmetric point in the contralateral skull.

tion. After the periosteum was unmasked, two burr holes were performed with a 1 mm dental drill in the calvaria, respectively, on the left and right sides, 3 mm lateral from the midline, 1 mm posterior to the bregma. Suspension ( $10 \mu\text{L}$ ) with  $1 \times 10^6$  C6 glioma cells were stereotactically injected at a depth of 5 mm, by a  $25 \mu\text{L}$  microamount syringe (the syringe was pricked 6 mm depth, and then was drawn 1 mm back) on the right side. The same volumes of sodium chloride were injected at the same depth on the left side. The holes were sealed with bone wax, and the operative field washed with saline solution and the skin sutured. The body temperature was maintained at  $37 \pm 0.5^\circ\text{C}$  using a homeothermic heating pad throughout the experiment. All the experimental procedures follow the institutional guidelines and were approved by the Southeast University, China.

### 2.3 NIRs and Experiments

NIR spectroscopy (NIRS) experiments were performed on POD 3, 10, and 17 with 10 rats each time. The homebuilt NIRs experimental system<sup>11</sup> includes a light source (HL-2000, Ocean Optics, Inc., Dunedin, FL), a bifurcated needle probe ( $600 \mu\text{m}$  o.d. with two single mode fibers of  $100 \mu\text{m}$ ), a spectrometer (USB 2000, Ocean Optics, Inc.), step motor and its driver system, a laptop, as shown in Fig. 1. The bifurcated needle probe is composed of two branches. One branch is connected to the light source and the other to the spectrometer. The backscattered intensity of light depends strongly on the absorption and scattering properties of the tissue. The optic fiber probe was held perpendicularly above the exposed calvaria surface and mounted on a step motor, which was attached to a stereotaxic frame. This step motor drives the fiber probe deep into the brain at an interval of 0.2 mm.

For data acquisition, LabView (National Instruments, Austin, TX) was used to program the interface between the spectrometer and the computer. The integration time, which was taken by the detector to read out the intensity of backscattered light, was kept constant at 100 ms during the entire set of measurements. The measurements were taken on the left and right brain. On each side, 40 steps in each brain side were measured, starting from the cortex with a spatial interval of 0.2 mm. The data were recorded for a period of 10 s at 2 Hz at each step.

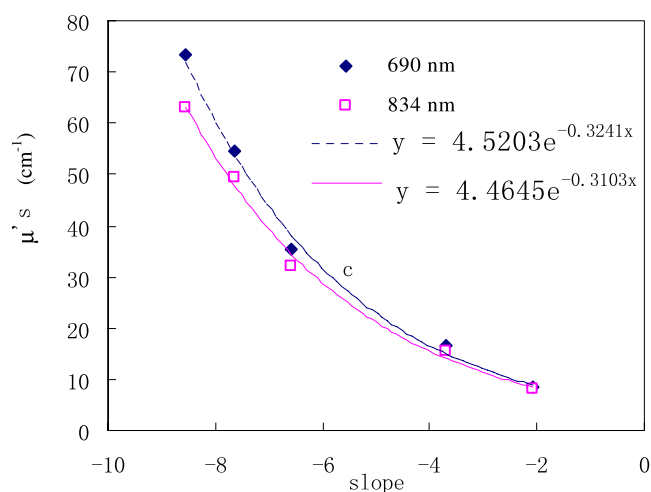


**Fig. 2** The reduced scattering coefficients from tissue simulation solution (intralipid) at 690 and 834 nm are shown with their slopes calculated from collected spectra of the same solutions. The coordinates of the y axis are  $\mu'_s$ , and the coordinates of the x axis are the slopes.

### 2.4 Calculating the Reduced Scattering Coefficient

The reduced scattering coefficient ( $\mu'_s$ ) serves as an index for the light-scattering property of the tissue. In principle, the intensity of backscattered light highly depends on light-scattering features of the tissue. Johns et al.<sup>5</sup> had found the slopes of reflectance spectra curves between 700 and 850 nm could be used to differentiate cerebral gray matter and white matter. Qian et al.<sup>11</sup> established a relationship among the reduced scattering coefficient, the profiles of the collected spectra from 700 to 850 nm, and the wavelength. In this study, an empirical formula between the reduced scattering coefficient and the slope between 700 and 850 nm was deduced by simulation experiment for the NIRs system before the rat experiments.

An intralipid solution of 8, 6, 4, 2, and 1% concentrations were chosen in the simulation experiment because these solutions yield light-scattering properties similar to those found in human tissues. The reduced scattering coefficients of these tissue simulation solutions (intralipid) were acquired by a standard Oximeter (model no. 96208, ISS, Inc., Illinois) working at 690 and 834 nm. At the same time, the reflectance spectra of these solutions were collected by the fiber-optic spectrometer of the NIRs system. Figure 2 shows the slopes and the relative reduced scattering coefficients.

The relationship between the slopes and the reduced scattering coefficients is obtained by the data fitting. Thus, an empirical formula for calculating the reduced scattering coefficient is derived as

$$\mu'_{s690} = 4.5203 \exp(-0.3241 * \text{slope}) \quad (1)$$

$$\mu'_{s834} = 4.4645 \exp(-0.3103 * \text{slope}). \quad (2)$$

The reduced scattering coefficients of intralipid solution measured by the Oximeter and calculated by Eqs. (1) and (2) and their differences are shown in Table 1, where the difference is equal to values calculated by the equations minus values measured by the Oximeter.

**Table 1** The reduced scattering coefficients of intralipid solution measured by Oximeter and calculated by Eqs. (1) and (2) and their differences.

| % Intralipid solution concentration | Slope | $\mu'_{s690}$ (cm <sup>-1</sup> ) |        |            | $\mu'_{s834}$ (cm <sup>-1</sup> ) |        |            |
|-------------------------------------|-------|-----------------------------------|--------|------------|-----------------------------------|--------|------------|
|                                     |       | Oxi-meter                         | Eq.(1) | Difference | Oxi-meter                         | Eq.(2) | Difference |
| 8                                   | -8.54 | 73.2                              | 72.0   | -1.2       | 63.2                              | 63.2   | 0.0        |
| 6                                   | -7.63 | 54.6                              | 53.6   | -1.0       | 49.4                              | 47.6   | -1.8       |
| 4                                   | -6.6  | 35.3                              | 38.4   | 3.1        | 32.1                              | 34.6   | 2.5        |
| 2                                   | -3.68 | 16.5                              | 14.9   | -1.6       | 15.3                              | 14.0   | -1.3       |
| 1                                   | -2.08 | 8.4                               | 8.9    | 0.5        | 8.1                               | 8.5    | 0.4        |

The accuracy of Eqs. (1) and (2) were further validated through the solid-tissue phantom experiment. Fifteen grams of Gelatin powder (Sigma, St Louis, MO, USA) made from porcine skin were added into 200 mL of boiling water and was dissolved completely by stirring. After the solution was cooled down, the intralipid solution with a certain concentration was added to the prepared gelatin solution. After that, the solution was frozen for the formation of the gelatin phantom. The percentage concentration of the intralipid used was varied, depending on the required  $\mu'_s$ . Five solutions with intralipid concentrations of 1–4% were used to create different  $\mu'_s$  values for gelatin phantoms, whose  $\mu'_{s690}$  and  $\mu'_{s834}$  measured by the Oximeter and calculated by Eqs. (1) and (2) and their differences are shown in Table 2.

It shows in Tables 1 and 2 that the maximum difference is 3.1 cm<sup>-1</sup> and mean difference at 690 nm is bigger than at 834 nm. The maximum difference at 834 nm is 2.5 cm<sup>-1</sup>. By combining the specific fiber-optic spectrometer with the empirical equations, an efficient method for real-time determination of the tissue reduced scattering coefficient is established.

## 2.5 Magnetic Resonance Imaging (MRI) and Histology Studies

MRI exams were performed at POD 10 and 17 on a 1.5-T MRI scanner (Philips Eclipse) using a human wrist coil after NIRs measurement. Gd-DTPA was applied intravenously at concentrations of 0.2 mmol/kg, 5 min before the scan. During the MRI scan, the rats were positioned in a plastic holder and anesthetized by 4% Nembutal (40 mg/kg, i.p.). Standard multislice sagittal and cross images were obtained by a TSE sequence with TR=4113 ms, TE=96 ms, NSA=2, FOV = 13 cm, slice thickness=3.0 mm, slice gap=0.5 mm, resolution=256 × 384, and seven slices.

After MRI, the rats were sacrificed with an anesthetic overdose and their brains were removed after the experiments. The brains were fixed in 10% formalin for more than 24 h and embedded in paraffin; consecutive 5  $\mu$ m coronal sections were cut and stained with hematoxylin and eosin. A semiquantitative assessment of pathology was carried out by the neuropathologist for each individual specimen.

**Table 2** The reduced scattering coefficients of gelatin phantoms measured by Oximeter and calculated by Eqs. (1) and (2) and their differences.

| % Intralipid concentration in phantoms | Slope | $\mu'_{s690}$ (cm <sup>-1</sup> ) |        |            | $\mu'_{s834}$ (cm <sup>-1</sup> ) |        |            |
|--|-------|-----------------------------------|--------|------------|-----------------------------------|--------|------------|
|  |       | Oxi-meter                         | Eq.(1) | Difference | Oxi-meter                         | Eq.(2) | Difference |
| 4                                      | -6.39 | 37.9                              | 35.9   | -2.0       | 30.7                              | 32.4   | 1.7        |
| 3                                      | -5.38 | 28.3                              | 25.8   | -2.5       | 22.4                              | 23.7   | 1.3        |
| 2.5                                    | -4.85 | 23.5                              | 21.8   | -1.7       | 19.6                              | 20.1   | 0.5        |
| 1.5                                    | -3.34 | 14.1                              | 13.3   | -0.8       | 11.9                              | 12.6   | 0.7        |
| 1                                      | -2.08 | 9                                 | 8.9    | -0.1       | 8.5                               | 8.5    | 0.0        |

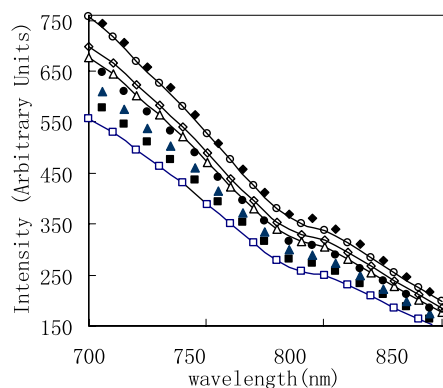


**Fig. 3** Reflectance spectra *in vivo* obtained from right side on POD 10 during experiment from 1 to 8 mm deep within the brain. Open square represents 1 mm deep. Filled square represents 2 mm deep. Open triangle represents 3 mm deep. Filled triangle represents 4 mm deep. Open diamond represents 5 mm deep. Filled diamond represents 6 mm deep. Open circle represents 7 mm deep. Filled circle represents 8 mm deep.

## 2.6 Statistical Analysis

The data reported here consist of only the reduced scattering coefficient at 690 and 834 nm. Spectral information between 700 and 850 nm for each sampling at each location in the brain was acquired. Data were collected 20 times at each measured point in a 10-s acquisition period and then averaged. The  $\mu'_s$  data finally used in this study were the data at each point. For each side of a rat brain, there were 40 values because the probe went 8 mm deep into the brain at an interval of 0.2 mm. The  $\mu'_s$  values were also averaged on 10 rats at each point of each side for POD 3, 10, and 17. Furthermore, all the 30 C6 glioma models were confirmed by the MRI and histology.

## 3 Results

### 3.1 Spectra and Light Scattering

Representative traces for the right brain (glioma) measured by the NIRS are shown in Fig. 3. They represent the different spectral value at different depths. The reduced scattering coefficients ( $\mu'_s$ ) at 690 and 834 nm were calculated by Eqs. (2.1) and (2.2) using these spectral slopes.

Analysis of  $\mu'_s$  showed that there were significant differences between left (control) and right (glioma) sides of the brain tissue (Fig. 4) on POD 10 and 17. Data in Fig. 4 are the average data at each point ( $n=20$ ).  $\mu'_{s690}$  versus depth have the same trend as  $\mu'_{s834}$  versus depth. It shows that  $\mu'_s$  of the right side within some range is lower than that of the left side at its corresponding position, and  $\mu'_s$  of POD 17 is lower than of POD 10 in the right side. On POD 10, there was significant difference between the left and right from a depth of 3.2 to 6.8 mm. On POD 17, the difference between the left and right is from a depth 1.2 to 7.2 mm. The  $\mu'_s$  values measured for the left (control) and right (glioma) brain side on POD 10 and 17 at depths of 1–8 mm are listed in Table 3 as mean  $\pm$  SEM, respectively.

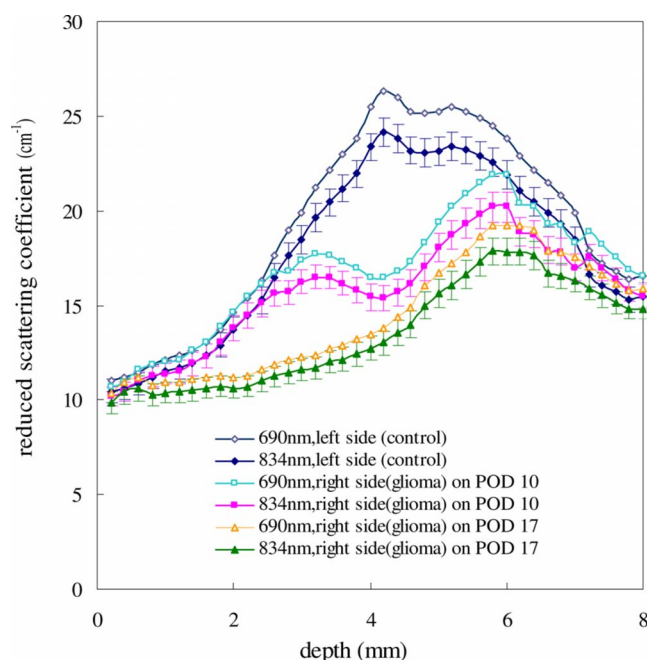


**Fig. 4**  $\mu'_s$  values for the left (control) and right (glioma) side from 0.2 to 8 mm deep within the brain. Open diamond represents 690 nm of the left side. Filled diamond represents 834 nm of the left side. Open square represents 690 nm of the right side on POD 10. Filled square represents 834 nm of the right side on POD 10. Open triangle represents 690 nm of the right side on POD 17. Filled triangle represents 834 nm of the right side on POD 17.

### 3.2 MRI Imaging

In images of T2-weighted spin-echo and gradient-echo with Gd-DTPA enhancement, there were ellipse high signals in the right hemisphere, and these high signals were inhomogeneous in some rats (Fig. 5).

### 3.3 Histology

The histopathological alterations of C6 gliomas were shown in Fig. 5. On a semiquantitative grading scale, all specimens had been classed into II/III grade by a neuropathologist. Prominent mitotic activity was observed under microscope on POD 10 [Fig. 6(a) and 6(b)], by which gliomas are classed into grade II. An amount of tumor cells necrosis and hemorrhage in the central region of tumors occurred on POD 17 [Fig. 6(c) and 6(d)], by which gliomas are classed into grade III.

## 4 Discussion

The *in vivo* measurements yielded  $\mu'_s$  to be within the range 11–26 and 10–24  $\text{cm}^{-1}$ , respectively, for 690 and 834 nm light in rat normal brain tissue, which is in good agreement with other *in vivo* measurements of  $\mu'_s$  in mammalian brains.<sup>12,13</sup> The upper and lower limits of the ranges can be taken as  $\mu'_s$  values of white matter and gray matter, respectively, at 690 and 834 nm, according to their depth distributions in rat brain. For glioma on POD 10, the mean  $\mu'_{s690}$  and  $\mu'_{s834}$  are 19.3  $\text{cm}^{-1}$  (standard error 1.8  $\text{cm}^{-1}$ ) and 17.9  $\text{cm}^{-1}$  (standard error 1.6  $\text{cm}^{-1}$ ), respectively. For glioma on POD 17, the mean  $\mu'_{s690}$  and  $\mu'_{s834}$  are 16.0  $\text{cm}^{-1}$  (standard error

**Table 3** The  $\mu'_s$  values for the left and right side on POD 10 and 17 at different deep within the brain ( $n=10$ ).

|                |        | $\mu'_s$ ( $\text{cm}^{-1}$ ) versus depth |                 |                 |                 |                 |                 |                 |                 |
|----------------|--------|--|-----------------|-----------------|-----------------|-----------------|-----------------|-----------------|-----------------|
|                |        | 1 mm                                       | 2 mm            | 3 mm            | 4 mm            | 5 mm            | 6 mm            | 7 mm            | 8 mm            |
| Left (690 nm)  |        | <b>12.1±2.9</b>                            | <b>14.6±3.3</b> | <b>19.9±4.8</b> | <b>25.5±5.2</b> | <b>25.2±5.7</b> | <b>23.8±5.4</b> | <b>19.9±5.2</b> | <b>16.5±4.6</b> |
| Right (690 nm) | POD 10 | 12.0±2.0                                   | 14.7±3.8        | 17.4±2.5        | 16.5±3.9        | 19.4±5.5        | 21.9±7.0        | 18.3±4.7        | 16.5±2.4        |
|                | POD 17 | 10.9±1.4                                   | 11.2±1.6        | 12.3±2.0        | 13.5±2.8        | 16.7±5.4        | 19.2±5.2        | 17.5±3.3        | 15.8±1.4        |
| Left (834 nm)  |        | <b>11.5±2.6</b>                            | <b>13.7±3.0</b> | <b>18.5±4.3</b> | <b>23.4±4.6</b> | <b>23.2±5.0</b> | <b>21.9±4.7</b> | <b>18.4±4.6</b> | <b>15.5±4.1</b> |
| Right (834 nm) | POD 10 | 11.4±1.8                                   | 13.8±3.4        | 16.2±2.2        | 15.4±3.5        | 18.0±4.9        | 20.2±6.1        | 17.0±4.1        | 15.5±2.1        |
|                | POD 17 | 10.4±1.3                                   | 10.6±1.4        | 11.6±1.8        | 12.7±2.5        | 15.6±4.8        | 17.8±4.6        | 16.3±2.9        | 14.8±1.2        |

$2.6 \text{ cm}^{-1}$ ) and  $15.0 \text{ cm}^{-1}$  (standard error  $2.3 \text{ cm}^{-1}$ ), respectively. To our knowledge, *in vivo* measurements of  $\mu'_s$  of glioma at these two wavelengths have not been reported.

Gliomas are neuroectodermal tumors. It induces perifocal edema and a massive increase of intracranial pressure for their compression, infiltration, and destruction of brain tissues. It was reported that glioma cells had abnormal chromosome and genetic expression, lower cytochrome-oxidase, creatine phos-

phate, adenosine triphosphate, and higher deoxyribonucleic acid than normal tissues.<sup>14-16</sup> In the SD C6 glioma model, significant loss of both the mitochondrial enzyme activity and the mitochondrial protein concentration were reported.<sup>7</sup>

In principle, scattering properties of tissues vary with the light-scattering media in tissues such as the cell membrane and organelle membrane,<sup>8</sup> the nuclei,<sup>17,18</sup> and other intracellular organelles, including the mitochondria.<sup>7,19-23</sup> Thus, light scattering can be a possible marker for tissue identification<sup>24-26</sup> and cancer diagnosis.<sup>6</sup> A lot of studies have documented that the scattering properties of gray and white matter in the brain differ significantly in the near-infrared range.<sup>5,12,27-30</sup> Recently, scattering properties are used to monitor and understand neuronal functions and physiological changes *in vitro* and *in vivo*.<sup>19,20,31,32</sup> It becomes a more recognized and frequently utilized research approach in the area of neuroscience.<sup>30-34</sup>

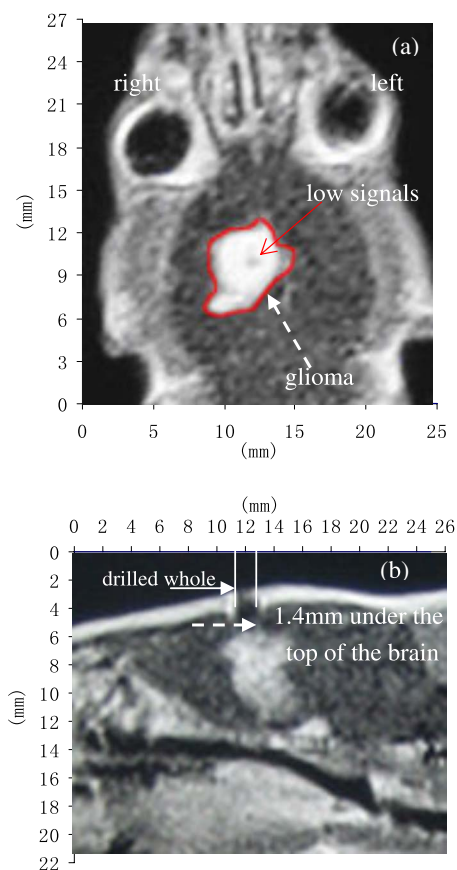


**Fig. 5** (a) Emerge low signals in the center of high signals, which represent necrosis or hemorrhage. (b) shows inhomogeneous high signal in the position where implant C6 glioma cells on POD 17.

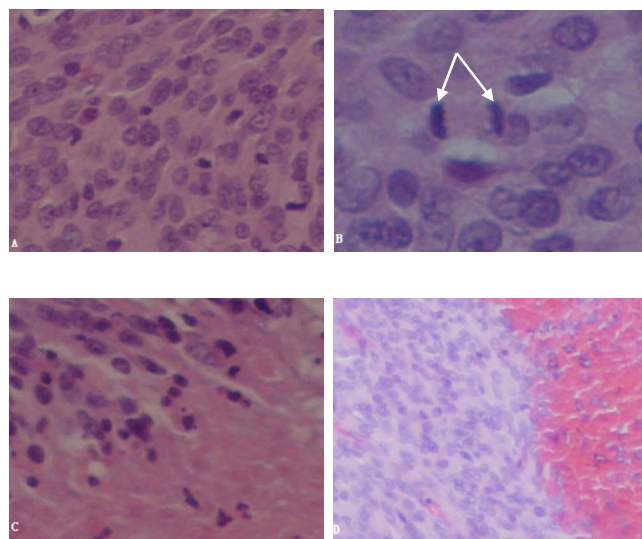


**Fig. 6** Microphotographs of C6 gliomas. A, C, D×200 E-H; B×400 E-H. (a) Shows grade I glioma (POD 10); (b) a mitotic phenomenon in the center of the photograph (arrows); (c) grade III, shows necrosis at low right; (d) grade III, hemorrhage in right side (POD 17).

Because cellular and intracellular organelles of tumors undergo changes in their density, morphological size, and shape, it is expected that light-scattering properties of tumors will differ from that of normal tissues. According to the existing reports,<sup>12,13,20,35–40</sup> the reduced scattering coefficients of tumors were found to be greater or less than normal tissues, dependent on tissue type and detecting wavelength. In this study, we cultured C6 cells to induce cerebral glioma in SD rats. The NIR spectra reflected from glioma were measured by NIRS to determine the reduced scattering coefficient. The results show the reduced scattering coefficient of glioma decreased compared to normal tissues at the same position, which is in good agreement with the 632 nm results reported by Angell-Petersen et al.<sup>13</sup>

The differences in reduced scattering coefficient observed in our *in vivo* data could be the mixed results of the following aspects:

1. Mitochondrial protein concentration:  $\mu'_s$  is found proportional to the mitochondrial protein concentration and decreases as the concentration falls.<sup>19</sup> Loss of mitochondrial protein concentration is found in glioma cells.<sup>7</sup>

2. Cell nuclei size: Mie theory predicts a general decrease in scattering, increase in anisotropy, and a subsequently large decrease in reduced scattering as the radius of tissue scatterer (cell nuclei, etc.) increases. Tumor cell nuclei are often larger than normal,<sup>41</sup> effectively decreasing the scattering from cell nuclei.

3. Cell nuclei density: The increased numbers of mitoses and multiple nuclei in a cell in tumors<sup>41</sup> act as additional scattering centers, which can partially offset the decrease in scattering.

4. Absorption: The signal obtained by our NIRS is somewhat influenced by total hemoglobin concentration, which usually increases three to five times as a tumor develops.<sup>18</sup> A simple experiment by adding two different concentrations of blood into 100 mL 4% intralipid solution was conducted.  $\mu'_{s690}$  and  $\mu'_{s834}$  measured by our NIRS decreased 1.3 and 1.1  $\text{cm}^{-1}$ , respectively, when total hemoglobin concentration increased from 13.4 to 59.7  $\mu\text{mol/L}$ . In the rat experiments,  $\mu'_{s690}$  and  $\mu'_{s834}$  decreased 5.8–8.5 and 5.2–7.6  $\text{cm}^{-1}$  in the center of the tumor (depth=5 mm), which shows absorption is not a main reason for  $\mu'_s$  changes observed in the rat experiments.

Although it is expected that the tissue undergoes disorganization within hours after C6 glioma implantation, we were unable to show such a change by the NIR technique on postoperative day 3. However, significant changes were found in our study on postoperative days 10 and 17, which correlate well with the expected pathological changes following glioma cells implantation. The following matters indicated the possibility by using *in vivo* NIR techniques to identify glioma. First, abnormal changes and their boundaries can be deduced by the  $\mu'_s$  curves. On the 10th day after C6 glioma cells were implanted at a depth of 5 mm in rat brain, there is significant difference between the left and right sides from depth 3.2 to 6.8 mm, which means the glioma enlarged, and depth 3.2 mm is its upper boundary and depth 6.8 mm is its lower boundary. On POD 17, the difference range between the left and right is from depth 1.2 to 7.2 mm, which means the volume of glioma is bigger. The upper boundary read from the

$\mu'_s$  curve is approximately consistent with the data read from MRI images. Second, the  $\mu'_s$  curves show the potential for differentiating a grading scale of gliomas. The histopathological alterations of C6 gliomas classified gliomas on POD 10 into grade II and gliomas on POD 17 into grade III. On the other hand, the  $\mu'_s$  of glioma side on POD 17 is lower than that on POD 10; that is,  $\mu'_s$  of gliomas of grade III is lower than grade II. However, more studies are needed to work out the differentiating number.

We did not observe the significant differences on POD 3. One possible explanation for the failure to detect the differences is due to the small volume of the glioma in its early stage. In the Sprague-Dawley rat C6 gliomas models, gliomas just begin to form a tumorous entity  $\sim 72$  h after the implantation.<sup>2</sup> Qian et al.<sup>42</sup> in previous research found that the probe used here has a look-ahead distance at  $\sim 1$  mm, which means the reduced scattering coefficient measured by this system is depending on the contribution of tissues located 1 mm under the probe. The percentage of intact versus diseased tissues in the 1 mm range may affect the scattering readings. It would be beneficial to develop a more sensitive NIR probe with a better spatial resolution. A second possibility may be the positioning of the NIR probe. A slight change in positioning angle could affect the reading. This possibility seems unlikely to account for a lack of group differences because there was no systematic difference in probe positioning. However, increased accuracy in probe positioning could be obtained by developing an optic digital scanner that could provide a measurement for the distance around the center of the aiming surface. Such information could feed back to a microprocessor, which would adjust the angle of the micromanipulator.

In conclusion, this study reports  $\mu'_s$  of normal brain tissue and glioma at two wavelength obtained using an NIRS method and demonstrates that NIRS has the ability to detect cerebral gliomas microinvasively. The results have proven our initial hypothesis and may suggest that the NIR techniques have a potential for intraoperative application to identify gliomas within normal brain tissue. We believe that such a minimally invasive technique with simple, low-cost, and portable aspects could be utilized for multiple applications in the brain and inner body-studies, such as to measure dynamic light scattering changes during external stimulations. The possibility of characterizing light scattering under tumors *in vivo* may allow scientists to gain insight into tumor physiology from another angle besides tissue hemoglobin oxygenation, which has been done intensively in recent years.

### Acknowledgments

This work was performed in Biophotonics Laboratory of Nanjing University of Aeronautics and Astronautics and supported by the National Nature Science Foundation of China (Grant No. 30671997).

### References

1. F. San-Galli, P. Vrignaud, J. Robert, J. M. Coindre, and F. Cohadon, "Assessment of the experimental model of transplanted C6 glioblastoma in Wistar rats," *J. Neuro-Oncol.* **7**(3), 299–304 (1989).
2. B. Grobden, P. De Deyn, and H. Slegers, "Rat C6 glioma as experimental model system for the study of glioblastoma growth and invasion," *Cell Tissue Res.* **310**(3), 257–270 (2002).

3. X. Zhu, C. Lu, B. Xiao, J. Qiao, and Y. Sun, "An experimental study of dendritic cells-mediated immunotherapy against intracranial gliomas in rats," *J. Neuro-Oncol.* **74**(1), 9–17 (2005).
4. G. H. Vince, M. Bendszus, T. Schweitzer, et al., "Spontaneous regression of experimental gliomas -An immunohisto chemical and MRI study of the C6 glioma spheroid implantation model," *Exp. Neurol.* **190**(2), 478–485 (2004).
5. M. Johns, C. A. Giller, and H. Liu, "Computational and *in vivo* investigation of optical reflectance from human brain to assist neurosurgery," *J. Biomed. Opt.* **3**(4), 437–445 (1998).
6. J. R. Mourant, I. J. Bigio, J. Boyer, R. L. Conn, T. Johnson, and T. Shimada, "Spectroscopic diagnosis of bladder cancer with elastic light scattering," *Lasers Surg. Med.* **17**(4), 350–357 (1995).
7. B. Beauvoit, S. M. Evans, T. W. Jenkins, E. E. Miller, and B. Chance, "Correlation between the light scattering and the mitochondrial content of normal tissues and transplantable rodent tumors," *Anal. Biochem.* **226**(1), 167–174 (1995).
8. J. Beuthan, O. Minet, J. Helfmann, M. Herrig, and G. Müller, "The spatial variation of the refractive index in biological cells," *Phys. Med. Biol.* **41**, 369–382 (1996).
9. F. W. Cheong, S. A. Prah, and A. J. Welch, "A review of the optical properties of biological tissues," *IEEE J. Quantum Electron.* **26**(12), 2166–2185 (1990).
10. V. M. Morreale, B. H. Herman, V. der Minassian, M. Palkovits, P. Klubes, D. Perry, A. Csiffary, and A. P. Lee, "A brain tumor model utilizing stereotactic implantation of a permanent cannula," *J. Neurosurg.* **78**(6), 959–965 (1993).
11. Z. Qian, R. Chen, Y. Gu, C. A. Giller, and H. Liu, "*In vivo* determination of tissue optical properties: reduced scattering coefficient ( $\mu_s$ 's)," *J. Nanjing Univ. Aeronaut. Astronaut.* **36**(3), 369–372 (2004).
12. F. Bevilacqua, D. Piguet, P. Marquet, J. D. Gross, B. J. Tromberg, and C. Depeursinge, "*In vivo* local determination of tissue optical properties: applications to human brain," *Appl. Opt.* **38**(22), 4939–4950 (1999).
13. E. Angell-Petersen, H. Hirschberg, and S. J. Madsen, "Determination of fluence rate and temperature distribution in the rat brain; implications for photodynamic therapy," *J. Biomed. Opt.* **12**(1), 014003 (2007).
14. M. E. Law, K. L. Templeton, G. Kitange, J. Smith, A. Misra, B. G. Feuerstein, and R. B. Jenkins, "Molecular cytogenetic analysis of chromosomes 1 and 19 in glioma cell lines," *Cancer Genet. Cytogenet.* **160**(1), 1–14 (2005).
15. S. Cazzaniga, S. C. Schold, H. D. Sostman, and H. C. Charles, "Effects of therapy on the  $^1\text{H}$  NMR spectrum of a human glioma line," *Magn. Reson. Imaging* **12**(6), 945–950 (1994).
16. M. S. Yang, L. C. Yu, and R. C. Gupta, "Analysis of changes in energy and redox states in HepG2 hepatoma and C6 glioma cells upon exposure to cadmium," *Toxicology* **201**(1–3), 105–113 (2004).
17. J. Ikeda, S. Terakawa, S. Murota, I. Morita, and K. Hirakawa, "Nuclear disintegration as a leading step of glutamate excitotoxicity in brain neurons," *J. Neurosci. Res.* **43**(5), 613–622 (1996).
18. K. Sokolov, R. Drezek, K. Gossage, and R. Richards-Kortum, "Reflectance spectroscopy with polarized light: is it sensitive to cellular and nuclear morphology," *Opt. Express* **5**(13), 302–317 (1999).
19. A. M. K. Nilsson, C. Stureson, D. L. Liu, and S. Andersson-Engels, "Changes in spectral shape of tissue optical properties in conjunction with laser-induced thermotherapy," *Appl. Opt.* **37**(7), 1256–1267 (1998).
20. G. Zonios, L. T. Perelman, V. Backman, R. Manoharan, M. Fitzmaurice, J. van Dam, and M. S. Feld, "Diffuse reflectance spectroscopy of human adenomatous colon polyps *in vivo*," *Appl. Opt.* **38**(31), 6628–6637 (1999).
21. B. Beauvoit, T. Kitai, and B. Chance, "Contribution of the mitochondrial compartment to the optical properties of the rat liver: A theoretical and practical approach," *Biophys. J.* **67**(6), 2501–2510 (1994).
22. C. A. Giller, M. Johns, and H. Liu, "Use of an intracranial near-infrared probe for localization during stereotactic surgery for movement disorders," *J. Neurosurg.* **93**(3), 498–505 (2000).
23. F. Fujii, Y. Nodasaka, G. Nishimura, and M. Tamura, "Anoxia induces matrix shrinkage accompanied by an increase in light scattering in isolated brain mitochondria," *Brain Res.* **999**(1), 29–39 (2004).
24. C. A. Giller, H. Liu, P. Gurnani, S. Victor, U. Yazdani, and D. C. German, "Validation of a near-infrared probe for detection of thin intracranial white matter structures," *J. Neurosurg.* **98**, 1299–1306 (2003).
25. F. Bevilacqua, "Local optical characterization of biological tissues *in vitro* and *in vivo*," Thesis/Dissertation, Swiss Federal Institute of Technology, 1998.
26. F. Bevilacqua, D. Piguet, P. Marquet, J. D. Gross, D. B. Jakubowski, V. Venugopalan, B. J. Tromberg, and C. Depeursinge, "Superficial tissue optical property determination using spatially resolved measurements close to the source: comparison with frequency domain photon migration measurements," *Proc. SPIE* **3597**, 540–547 (1999).
27. F. A. Duck, *Physical Properties of Tissue: A Comprehensive Reference Book* Academic Press, San Diego (1990).
28. E. Okada, M. Firbank, L. J. Johnson, S. R. Arridge, M. Cope, and D. T. Delpy, "Theoretical and experimental investigation of near-infrared light propagation in a model of the adult head," *Appl. Opt.* **36**(1), 21–31 (1997).
29. L. J. Johnson, D. F. Hanley, and N. V. Thakor, "Optical light scatter imaging of cellular and sub-cellular morphology changes in stressed rat hippocampal slices," *J. Neurosci. Methods* **98**(1), 21–31 (2000).
30. P. G. Aitken, D. Fayuk, G. G. Somjen, and D. A. Turner, "Use of intrinsic optical signals to monitor physiological changes in brain tissue slices," *Methods* **18**(2), 91–103 (1999).
31. B. S. Kristal and J. M. Dubinsky, "Mitochondrial permeability transition in the central nervous system: induction by calcium cycling-dependent and independent pathways," *J. Neurochem.* **69**(2), 524–538 (1997).
32. R. D. Andrew, C. R. Jarvis, and A. S. Obeidat, "Potential sources of intrinsic optical signals imaged in live brain slices," *Methods* **18**(2), 185–196 (1999).
33. M. Haller, S. L. Mironov, and D. W. Richter, "Intrinsic optical signals in respiratory brain stem regions of mice: neurotransmitters, neuromodulators, and metabolic stress," *J. Neurophysiol.* **86**, 412–421 (2001).
34. Y. Nomura, F. Fujii, C. Sato, and M. Tamura, "Exchange transfusion with fluorocarbon for studying synaptically evoked optical signal in rat cortex," *Brain Res. Brain Res. Protoc.* **5**(1), 10–15 (2000).
35. S. C. Gebhart, W. C. Lin, and A. Mahadevan-Jansen, "In vitro determination of normal and neoplastic human brain tissue optical properties using inverse adding-doubling," *Phys. Med. Biol.* **51**(8), 2011–2027 (2006).
36. P. R. Bargo, S. A. Prah, T. T. Goodell, R. A. Steven, G. Koval, G. Blair, and S. L. Jacques, "*In vivo* determination of optical properties of normal and tumor tissue with white light reflectance and an empirical light transport model during endoscopy," *J. Biomed. Opt.* **10**(3), 034018 (2005).
37. J. P. Ritz, C. M. Isbert, A. Roggan, C. T. Germer, G. Mueller, and H. J. Buhr, "Correlation of intrahepatic light and temperature distribution in laser-induced thermotherapy of liver tumors and liver tissue," *Proc. SPIE* **3565**, 18–23 (1999).
38. C. Holmer, K. S. Lehmann, J. Wanken, C. Reissfelder, A. Roggan, G. Mueller, H. J. Buhr, and J. P. Ritz, "Optical properties of adenocarcinoma and squamous cell carcinoma of the gastroesophageal junction," *J. Biomed. Opt.* **12**(1), 014025 (2007).
39. D. Grosenick, K. T. Moesta, M. Moller, et al., "Analysis of time-domain optical mammograms recorded from more than 150 patients," *Proc. SPIE* **5693**, 308–317 (2005).
40. S. S. Barbour, R. L. Barbour, P. C. Koo, H. L. Graber, and J. Chang, "Mapping of photon distribution and imaging of MR-derived anatomically accurate optical models of the female breast," *Proc. SPIE* **2389**, 835–850 (1995).
41. D. Schiffer, *Brain Tumors: Biology, Pathology and Clinical References*, Springer, Berlin (1997).
42. Z. Qian, S. V. Sunder, Y. Gu, C. A. Giller, and H. Liu, "Look-ahead distance of a fiber probe used to assist neurosurgery: Phantom and Monte Carlo study," *Opt. Express* **11**(16), 1844–1855 (2003).